THE JOURNAL OF PHYSICAL CHEMISTRY B

Article

pubs.acs.org/JPCB

Exploring the Diffusion of Molecular Oxygen in the Red Fluorescent Protein mCherry Using Explicit Oxygen Molecular Dynamics Simulations

Chola K. Regmi, Yuba R. Bhandari, Bernard S. Gerstman, and Prem P. Chapagain*

Department of Physics, Florida International University, Miami, Florida 33199, United States

Supporting Information

ABSTRACT: The development of fluorescent proteins (FPs) has revolutionized cell biology research. The monomeric variants of red fluorescent proteins (RFPs), known as mFruits, have been especially valuable for tagging and tracking cellular processes in vivo. Determining oxygen diffusion pathways in FPs can be important for improving photostability and for understanding maturation of the chromophore. We use molecular dynamics (MD) calculations to investigate the diffusion of molecular oxygen in one of the most useful monomeric RFPs, mCherry. We describe a pathway that allows oxygen molecules to enter from the solvent and travel through the protein barrel to the chromophore. We calculate the free-energy of an oxygen molecule at points along the path. The pathway contains several oxygen hosting pockets, which are identified by the amino acid residues that form the pocket. We also investigate an RFP variant known to be significantly less photostable than mCherry and find much easier oxygen access in this variant. The results provide a better understanding of the mechanism of molecular oxygen access into the fully folded mCherry protein barrel and provide insight into the photobleaching process in these proteins.

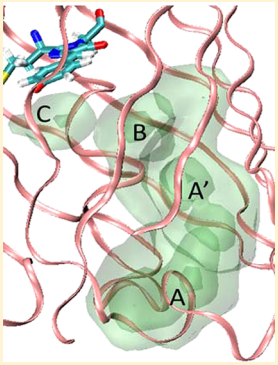

INTRODUCTION

The development of fluorescent proteins (FPs) has revolutionized cell biology research.[1−3] The monomeric variants of red fluorescent proteins (RFPs), known as mFruits,[4] have been especially valuable as markers for in vivo applications in mammalian cell imaging.[5] The development of these mutant monomeric variants avoids the issues of oligomerization[6,7] that occur in naturally occurring FPs with emission peaks in this region of the spectrum. The polymeric structure of naturally occurring RFPs, such as DsRed, interferes with their use in tagging purposes because oligomeric FPs and aggregates[8] can result in significant perturbations to normal cellular activities. Monomeric mFruits have found increasing applications in recent years. Long-term imaging applications of fluorescent proteins could be expanded through the development of variants with higher photostability. Better shielding of the chromophore from the environment, as well as reducing the access of molecular oxygen to the chromophore, has been shown to significantly increase the photostabilities of both GFPs and RFPs.[9] The Q64H and F99Y mutations introduced in mOrange resulted in the significantly more photostable mOrange2, possibly by these mutations helping to block the detrimental oxidation step by rearranging the protein−chromophore environment.[10] This suggests that the irreversible photobleaching is enhanced due to the diffusion of molecular oxygen through the protein barrel surface[6] into the protein interior, in addition to the irreversible photobleaching from transient dark states produced by photoisomerization or excited state proton transfer. Also, since chromophore formation in FPs requires access to molecular oxygen, understanding oxygen diffusion pathways in FPs is important from the perspectives of both photostability and chromophore maturation.

Recent investigations have shown that protein flexibility plays a major role in gas access into many proteins.[11−16] Conformational flexibility of the side chains of the residues involved in forming transient cavities or pathways can alter the sizes of the bottlenecks for gas diffusion, as well as changing the gating mechanism at the protein surface.[17−21] In FPs, in addition to affecting the structures of both the chromophore and the protein barrel,[22] the chromophore−barrel interaction can also affect the fluctuations of the barrel, which in turn can modify the spectral properties and lifetime of the fluorescence.[23] It is shown in a recent important work on cyan fluorescent protein that the reduction in the flexibility of a beta strand in the barrel has led to a dramatic improvement in fluorescence quantum yield.[24]

In an important work,[25] Roy et al. investigated the diffusion pathways of oxygen in the phototoxic KillerRed protein. In this protein, reactive oxygen is generated from molecular oxygen that diffuses into the interior of the protein. They were able to identify the pores and channels for the oxygen to escape through the protein barrel to the bulk solvent. This study also suggested that the ease of molecular oxygen diffusion through a channel is the cause of the high susceptibility for photobleaching.[25] In our earlier work (ref 26), oxygen diffusion pathways in mCherry were investigated by implicit ligand sampling techniques. In that study, an immature tripeptide

Received: August 22, 2012
Revised: January 23, 2013
Published: January 30, 2013

   dx.doi.org/10.1021/jp308366y | J. Phys. Chem. B 2013, 117, 2247−2253

form of the chromophore was used, and crystallographic water molecules were not included in order to quicken barrel fluctuations so that they could be observed in shorter simulation time scales. To better understand the diffusion process in a more realistic setting, in work reported here we have performed molecular dynamics (MD) simulations with explicit molecular oxygen in the system. We use force field parameters for a mature chromophore and also include the crystallographic water in the simulations. The results of these computations describe a pathway that allows oxygen molecules to enter from the solvent and travel through the protein. The pathway contains several oxygen hosting pockets, which are identified by the amino acid residues that form the pocket. We calculate the free-energy of an oxygen molecule at any point along the path. The results provide a better understanding of the mechanism of molecular oxygen access into the fully folded mCherry protein barrel and provide insight into the photobleaching process in these proteins.

METHODS

Molecular Dynamics. Time series trajectories were obtained from explicit solvent, all-atom simulations using the NAMD molecular dynamics package with the CHARMM27 force field.[27] The initial X-ray crystallographic structures of RFP mCherry (pdb code 2H5Q) was obtained from the Protein Data Bank, and the missing amino acid residues were inserted using MODELER.[28] Force field parameters for the mature chromophore were adopted from the anionic GFP chromophore developed by Reuter et al.[29] and from CHARMM27 parameters for acylimine nitrogen. Throughout the simulation, the deprotonated anionic form of the chromophore in the ground state was used. In addition, Glu215 was protonated using a patch.

The VMD package was used to setup the system for simulations. The initial structure of mCherry with crystallographic water molecules and one molecular oxygen was solvated by using the *solvate* plugin in VMD. Using a box cutoff of 10 Å, the dimensions of the simulation box were 83.3 × 75.6 × 63.4 Å^3. The solvated system was electrically neutralized by adding six Na^+ ions randomly in the bulk water using the VMD *autoionize* plugin. The final system contained a total of 37 276 atoms. All water molecules overlapping with the protein were removed. The particle mesh Ewald method[30] was used to treat long-range interactions with a 12 Å nonbonded cutoff. Energy minimization was performed using the conjugate gradient and line search algorithm. The system was then heated with a linear gradient of 20 K/ps from 20 to 300 K. At 300 K, the system was equilibrated for 15 ps with a 2 fs integration time step in the NVT (constant number, volume, and temperature) ensemble. Langevin dynamics was used to maintain the temperature at 300 K. An 80 ns NVT dynamics simulation with 2 fs time steps was used for analysis.

Locally Enhanced Sampling (LES) for Molecular Oxygen. We performed explicit oxygen simulations to determine the locations of specific pathways for oxygen diffusion and quantify their transport properties. For explicit oxygen simulations, oxygen molecules were included during the MD simulations. A locally enhanced sampling (LES) technique[31] was employed to enhance the statistics for the diffusion of the molecular oxygen. In this method, an oxygen molecule was first placed in the solvated box near the protein barrel. The *psfgen* plugin implemented in VMD was used to generate a total of 15 noninteracting copies of the O_2 molecule for enhanced searching for diffusion pathways. Simulations were performed with no biasing force or potential that might facilitate oxygen entry into the interior.

Implicit Ligand Sampling (ILS) for Molecular Oxygen. Implicit ligand sampling (ILS)[31] was employed to quantify the properties of oxygen diffusion pathways. ILS computations calculate the potential of mean force (PMF) corresponding to the placement of a given small ligand such as O_2, anywhere inside the protein. The calculated PMF provides the Gibb's free-energy cost of having a particle located at a given position and quantifies the area accessible to the ligand. We applied PMF/ILS calculations to the protein conformations in the frames of our MD simulations to determine locations in the protein that are especially important for blocking or facilitating oxygen passage and to quantify the free-energy differences at these locations. A total of 5000 protein conformations from a 10 ns MD trajectory were used for ligand sampling. Therefore, the free-energy value at each of the locations is the average obtained from the ILS performed every 2 ps for the 10 ns MD trajectory. In performing the free-energy calculations at each O_2 location, 20 different rotational orientations of molecular dioxygen were sampled at each gird position. The volume element size of the grid was 1 Å^3.

The free-energy values are calculated relative to a dioxygen molecule placed outside the protein in the surrounding water, where the free-energy is defined to be zero. The values of the free-energy along the diffusion pathway reaction coordinate were calculated for positions separated by approximately 1 Å distance, extending from the solvent outside the protein, and through the protein leading to the chromophore. The pathways were determined from visual inspection as well as from the 3D grid data of free-energy values from ILS simulations.

RESULTS AND DISCUSSION

Structural Features of mCherry. The first monomeric variant of the red fluorescent protein, mRFP1 was derived from the Discosoma sp. fluorescent protein DsRed.[4,32] Development of the monomeric RFP overcame the problems of tetramerization and slow maturation of the parent protein DsRed. However, mRFP1 suffered from lower quantum yield and lower photostability, possibly due to the compromised barrel structure caused by the mutations introduced to break the tetramer interactions at the interface. The monomeric variant mCherry is one of the next-generation monomeric RFPs derived from mRFP1 and has significantly improved photophysical properties.[4] Among the mutations introduced to obtain mCherry, Q66M enhanced the maturation, V7I and M182K enhanced the folding, and M163Q removed an unwanted absorbance peak, in addition to significantly enhancing the mCherry photostability.[10] As discussed later, our simulation results show that the M163Q mutation in mCherry significantly reduces molecular oxygen entry into the barrel, which might help explain the role of molecular oxygen in permanent photobleaching of FPs and improving the photostability in mCherry.

As with other mFruit variants, the barrel structural integrity is compromised, especially in the β7 and β10 region, due to missing tetrameric interactions present in the naturally occurring DsRed. Transient thermal fluctuations[26] can allow easier oxygen access to the chromophore. This may help chromophore maturation but can cause fluorescence quenching or faster photobleaching due to oxidation. In cyan fluorescent protein, β7 flexibility has been attributed to cause collisional

dx.doi.org/10.1021/jp308366y | J. Phys. Chem. B 2013, 117, 2247−2253

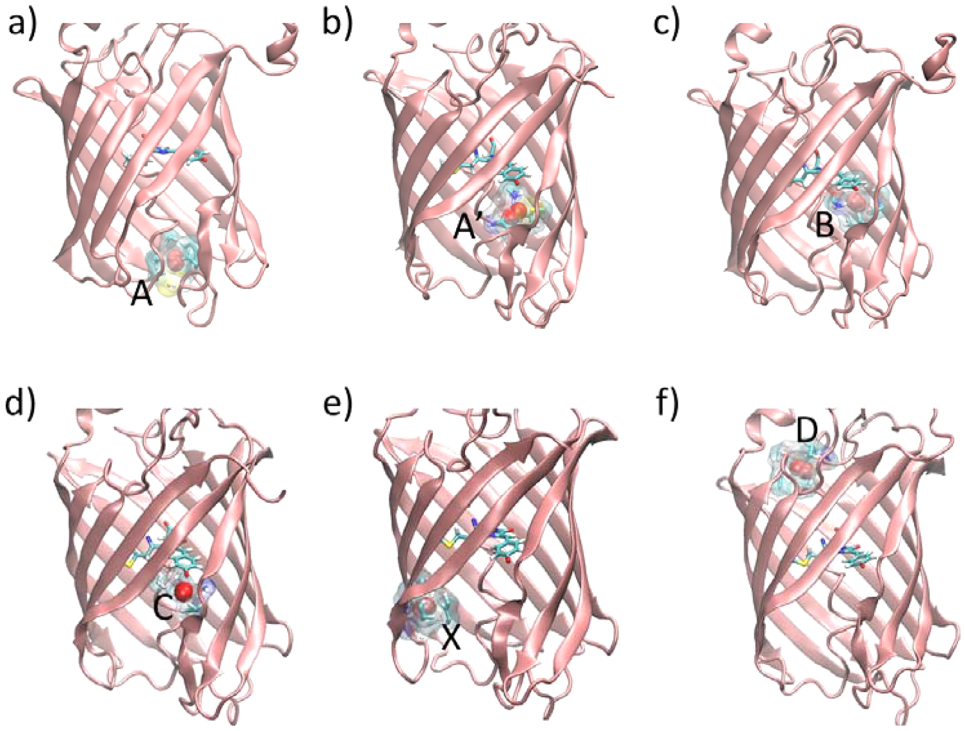

Figure 1. Various oxygen-hosting pockets in the mCherry protein barrel. (a–d) Pockets A, A′, B, and C are part of the same oxygen diffusion channel. Pocket C is in the vicinity of the chromophore. Other pockets exist (X and D) but do not connect to the channel. (e) Pocket X close to the middle of the barrel but off to the side (f) pocket D near the top of the barrel.

fluorescent quenching due to the collision of the Ile146 side chain with the chromophore. In a recent work, structure guided amino acid replacements to reduce β7 flexibility have led to a significantly brighter and highly photostable fluorescent protein mTurquoise2, with the highest quantum yield (93%) among monomeric fluorescent proteins.[24]

In ref 26, the barrel structure of mCherry is compared with that of citrine. Implicit oxygen ligand sampling showed that the β7–β10 gap in mCherry provides an easy path for oxygen entry. In addition, static structural comparison also shows differences at the top and the bottom of the barrels. For example, the top of the citrine barrel contains an extra α-helix, which is not present in mCherry. In this region of mCherry, there is a random coil (or loop segment), and therefore, larger structural fluctuation can be expected. In the earlier study with implicit ligand sampling, no clear entry path for oxygen was observed from the top of the barrel. However, this does not conclusively prove that an oxygen pathway does not exist because implicit ligand sampling may not capture a dynamic pathway that opens and closes but with gatekeeping amino acids that open for a very short time. Moreover, the presence of an actual oxygen molecule can slightly modify the environment in a way that might allow the oxygen to enter the protein barrel. The explicit oxygen simulations carried out in the present investigations are able to capture these possibilities.

Molecular Oxygen Diffusion Pathways in mCherry. For enhanced search statistics, our explicit oxygen calculation employed 15 copies of oxygen in our NAMD LES calculations. The oxygen molecules do not interact with each other, but interact with the rest of the system. With these 15 copies of noninteracting oxygen molecules in the system, we performed an 80 ns production run. The simulations reveal several different types of events of molecular oxygen entry into the protein barrel from various locations, which are pictured in Figure 1 and described below. We observed several protein pockets far from the chromophore where the molecular oxygen can enter and remain for an extended time. Some of these pockets are dead-ends with no access to the chromophore, but some of the pockets join to pathways that ultimately lead to the chromophore.

Diffusion of Oxygen into Pockets Far from the Chromophore. In our simulations, the first oxygen entry occurred at the bottom of the barrel at approximately 4 ns into the production run. This oxygen-hosting pocket is formed by the side chains of PHE56, ILE60, PHE129, and MET136. We label this pocket as pocket A and display it in Figure 1a. Oxygen enters this pocket through residues HIS25, PRO55, and MET136, which act as gateway residues for multiple entries and exits of the oxygen molecules. It is found that the oxygen can also enter pocket A through residues PRO134 and TYR173. Entry through this gate took 5 ns to reach pocket A.

We focus our attention on the gate composed of residues HIS25, PRO55, and MET136. The first oxygen that enters at 4 ns escapes back to the solvent after only 200 ps in the pocket. However, another O_2 molecule enters again through this gate at 10 ns. This time, the oxygen stays in the pocket for approximately 1 ns and then moves further into the protein to a second pocket (pocket B) formed by residues GLN64, ARG95, MET97, and VAL105 as shown in Figure.1c. Multiple back and forth transitions of the oxygen between pockets A and B were observed. These transitions are shown in Figure 2, which displays the distance of the oxygen molecule from a reference point on the chromophore. We chose nitrogen N3 of the imidazoline ring as the reference point because this part of the chromophore is least flexible. The oscillations of the oxygen (red) between pockets A and B occurs rapidly and shows no intermediate pocket. During further simulations, we observed a different oxygen molecule enter pocket A and also make back

dx.doi.org/10.1021/jp308366y | J. Phys. Chem. B 2013, 117, 2247–2253

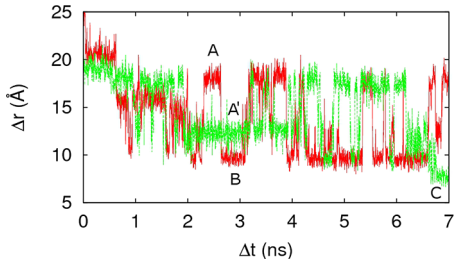

Figure 2. Trajectories of molecular oxygen showing its distance from the chromophore for a 7 ns window. One trajectory (red) involves oscillations between two pockets in the protein (pockets A and B of Figure 1). The other trajectory (green) involves oscillation between the same two pockets, but also includes oxygen movement in an intermediate pocket, pocket A′ of Figure 1b, and to pocket C close to the chromophore. The starting point $\Delta t = 0$ corresponds to 52 ns into the simulation for the green trajectory and 66 ns for the red trajectory.

and forth transitions between pockets A and B, but via an intermediate pocket (pocket A′ of Figure 1b) formed by residues LEU61, MET97, LEU124, T127, and GLY126. The MET97 side chain forms a part of both pockets A′ and B, so the movement of this side chain allows the transition between these pockets. Figure 2 shows a second trajectory (green) for an oxygen movement that occurs via an intermediary pocket (pocket A′). Ultimately, this oxygen molecule makes the transition to pocket C (Figure 1d) and then escapes the protein barrel (Supplementary Movie S1) as described later. In the 7 ns time window shown in Figure 2, only the second trajectory (green) includes an oxygen transition to pocket C, whereas the first trajectory (red) shows oscillations between pockets A and B only. Supplementary Movie S1 shows approximately the last 4 ns of the green trajectory.

An interesting pocket (pocket X of Figure 1e) observed during the simulation is formed by residues LEU46, VAL48, TYR208, THR209, and VAL211 and lies in the barrel interior but off to a side, close to the β3 and β11 strands of the barrel. This mostly hydrophobic pocket hosts the oxygen for a very long time. Oxygen is observed to enter this pocket at 34 ns and remain there for the rest of the 80 ns simulation. Although the oxygen in this pocket is far from the chromophore, 18 Å from the phenolate oxygen, and is not part of any oxygen diffusion channel, we cannot rule out the possibility that an oxygen in this pocket can affect the chromophore, especially since it stays in the pocket for tens of nanoseconds. Another pocket (pocket D, Figure 1f) was observed near the top of the barrel and is formed by residues ILE8, PRO37, ALA71, TYR72, and PHE118, with the side chain of TYR72 blocking the oxygen from diffusing further into the barrel. All of these residues are conserved in the mFruits. An oxygen that enters pocket D escapes back to the solvent in less than a nanosecond via the same route that it entered. This pocket may be important because oxygen enters and leaves this pocket multiple times.

We also observed a transient cavity at the barrel surface that is formed by the side chains of LEU54, PHE56, TRP58, and LEU61. These amino acids belong to the central α-helix inside the barrel. The oxygen enters this cavity at 9 ns and escapes back to the solvent at 10 ns. No pathways to the chromophore or to other pockets are found, so an oxygen molecule that enters this cavity will quickly escape to the solvent. The side chain of LEU61 separates the chromophore from this cavity, and therefore, this residue plays a crucial role in preventing the oxygen from reaching the chromophore. Comparison of amino acid sequences shows that these four amino acids are conserved throughout the mFruit family, as well as the parent DsRed. Except for LEU54, the other three amino acid residues are also conserved in GFP.

Diffusion of Oxygen into Pockets in the Vicinity of the Chromophore. The β7−β10 region of the barrel is important for oxygen entry because the β7−β10 gap undergoes thermal fluctuations that repeatedly produce a large opening. The amino acid residues near this gap, TRP143 of β7, GLN163 of β8, and LEU199 of β10, form a small gateway pocket just inside the surface. This gateway pocket is important because it provides access both to the chromophore and to other pockets further inside the protein, but it is transient, depending on the fluctuations of β7 and β10. Later in this article, we focus our attention on residue 163 because the side chain of GLN163 is found to be responsible for hindering the diffusion of molecular oxygen further into the barrel. This provides a possible molecular basis for the improved photostability in mCherry, as compared to its predecessor variant, which has MET163 at that position.

In order to investigate the β7−β10 gateway pocket in more detail, we cut out uninteresting computational time during which the oxygen molecule moved around in the solvent outside the protein. The initial entry of an oxygen molecule from the solvent into this gateway pocket required 71 ns. In order to avoid the computational wait-time for the oxygen in the solvent to get to the gate point between β7−β10, we ran 20 new simulations. Instead of LES with 15 different oxygen molecules, we used 20 independent simulations, each with just one oxygen molecule placed at the β7−β10 gate. This expedited the search for pathways into the protein through the β7−β10 gate. A simulation was terminated if the oxygen molecule escaped the protein and went out to the solvent. We considered the oxygen molecule to have completely escaped and terminated the simulation run if the oxygen's distance from the chromophore's phenolate oxygen exceeded 15 Å. This distance ensures that a simulation will not be terminated if the oxygen has not truly escaped the β7−β10 gate and an oxygen that remains in the vicinity just outside the pocket will be given time to reenter. In nine runs, the oxygen molecule escaped immediately (within picoseconds). In the other 11 of these 20 simulations, the oxygen molecule entered completely into the gateway pocket. For 10 of these 11 simulations, the oxygen molecule remained in the pocket for 13 ns on average, before escaping back into the solvent. Only in one simulation did the oxygen molecule manage to diffuse further into another pocket, pocket C shown in Figure 1d and Supplementary Movie S2.

Pocket C is formed by several amino acids including ARG95, MET97, TRP143, GLN163, and VAL177. This pocket is especially important because it is very close to the chromophore (just below the chromophore). As we show later, a mutation of GLN163 allows easier entry for the molecular oxygen from the gateway pocket to pocket C.

Oxygen Diffusion Channels Connecting Multiple Pockets. Analysis of the trajectories of individual oxygen molecules showed two vulnerable regions of the protein through which molecular oxygen can enter and ultimately reach pocket C, which is directly underneath the chromophore. As described above, one of these regions on the barrel close to pocket C is a gap on the surface between strands β7 and β10. The other entry region is near pocket A and further away from the chromophore. Residues HIS25, PRO55, MET136, PRO134,

dx.doi.org/10.1021/jp308366y | J. Phys. Chem. B 2013, 117, 2247−2253

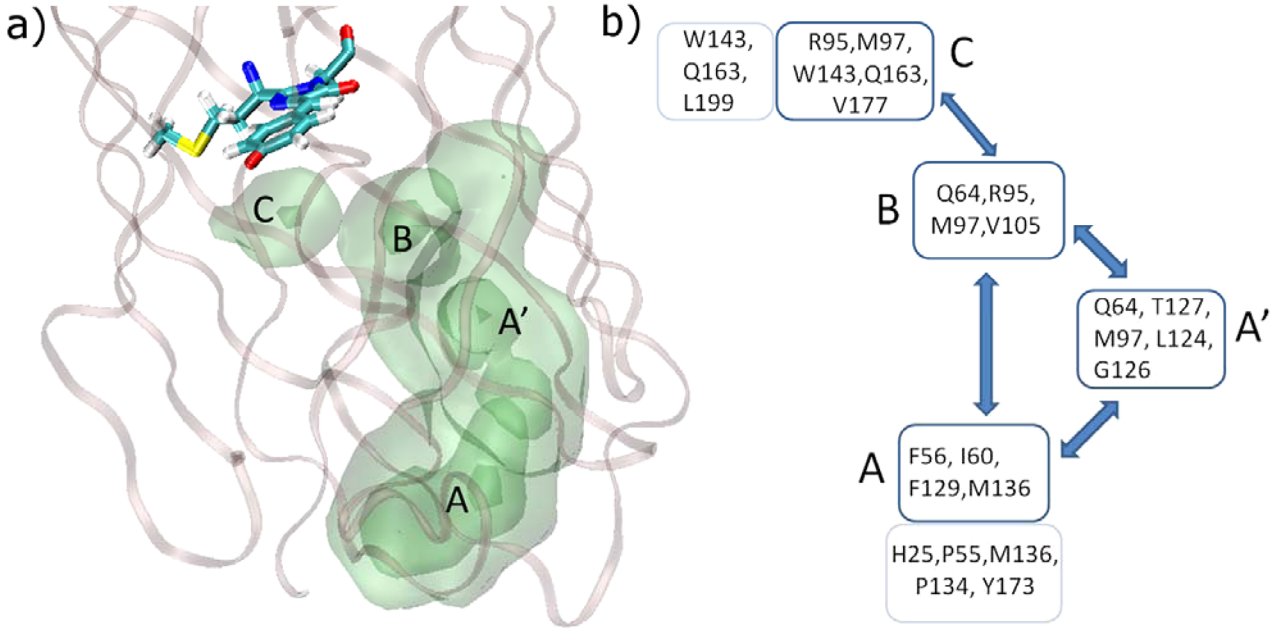

Figure 3. (a) Volumetric trace of the oxygen diffusion channel from one side of the protein to the other. (b) Amino acid residues involved in the oxygen diffusion channel. Common amino acid residues shared by different pockets indicate that the side chains of these residues separate the pockets. In addition to the amino acids involved in defining the different pockets, the gateway residues are also shown in light colored boxes just outside pockets A and C.

and TYR173 act as the gateway residues in this region (near pocket A).

A complete passage of an oxygen molecule that enters from one side of the protein and leaves through the other side (solvent → pocket A ↔ B → pocket C→ $\beta7-\beta10$ gateway pocket → solvent) was observed from 51 to 63 ns of simulation. During this time, we also observed the diffusion of oxygen between pocket A ↔ pocket A′. The reverse pathway was observed at 71 ns in which an oxygen molecule entered through the gap between $\beta7-\beta10$ and traveled a path from solvent → $\beta7-\beta10$ gateway pocket → pocket C → pocket B → pocket A → solvent. The oxygen molecule that entered the barrel at 71 ns through $\beta7-\beta10$ ultimately escaped from the bottom of the barrel at 73 ns. This pathway is a complete channel from the $\beta7-\beta10$ gateway near pocket C into the barrel interior and then exiting near pocket A. Figure 3 summarizes the pathways and the residues involved in forming the channel for oxygen diffusion from one side of the protein to the other.

Free-Energies along the Pathway Calculated from Implicit Ligand Sampling. We performed implicit ligand sampling to calculate the free-energy of an oxygen molecule at positions along the channel displayed in Figure 3. Figure 4 displays the free-energy along a reaction coordinate that represents the oxygen diffusion pathway (channel), which allows an oxygen molecule in the solvent to enter the protein and approach the chromophore. The free-energy curve in Figure 4 is based upon reaction coordinate points that are at 1 Å separations along the channel. There are clear free-energy minima for pockets A, B, and C. The barrier between pockets A and B is relatively small, which indicates that it is relatively easy for the oxygen to move back and forth between these pockets. This is consistent with the short oscillation times displayed in the red curve of Figure 2. In contrast, the barrier between pockets B and C is much higher. The high free-energy barrier makes it more difficult for the oxygen molecule to travel

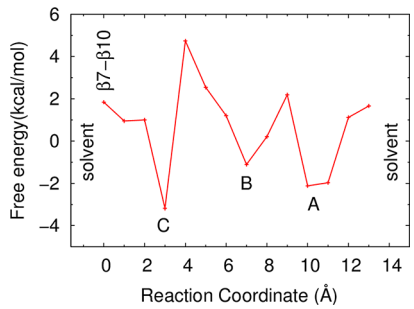

Figure 4. Free-energy values for the oxygen molecule at locations along the curved pathway (channel) of Figure 3 connecting the solvent and the protein interior. The reaction coordinate is the distance of the oxygen molecule with respect to the chromophore.

between these pockets. During the 80 ns LES simulation, we only observed a total of three B ↔ C barrier crossing events: two from pocket B to pocket C and one from pocket C to pocket B.

M163Q Mutation and the Enhanced Photostability of mCherry. During the directed evolution of mCherry from mRFP1, the mutation M163Q was experimentally determined to be solely responsible for enhanced photostability in mCherry.[10] In order to understand the role of molecular oxygen in fluorescent protein photostability, we performed simulations with the reverse mutation Q163M in mCherry and investigated the oxygen diffusion pathways in the mutant mCherry−Q163M. We performed both LES as well as a number of independent simulations. A 30 ns LES simulation with 15 copies of molecular oxygen was performed. As with the mCherry simulations, the 15 copies were placed just outside the protein barrel. Within the 30 ns simulation, we observed a total of five molecular oxygen entries into the barrel, three through the gateway pocket near the $\beta7-\beta10$ gap, and two from the bottom of the barrel. (In contrast, there was no molecular

dx.doi.org/10.1021/jp308366y | J. Phys. Chem. B 2013, 117, 2247−2253

oxygen entry into the mCherry barrel through the gateway pocket near the $\beta7-\beta10$ gap until 71 ns.) The first close approach of molecular oxygen to the chromophore in mCherry−Q163M occurs fairly quickly, at 11 ns, and this oxygen enters through the gateway pocket near the $\beta7-\beta10$ gap. The distance of closest approach between the phenolic oxygen in the chromophore and the molecular oxygen was 2.5 Å. The oxygen molecule then quickly transitions further into pocket C.

In two other oxygen entries (at 14 and 26 ns) through this gateway pocket in mCherry−Q163M, the molecular oxygen continued diffusing further into the protein but through a new route, not observed in mCherry. Rather than diffusing into pocket C, these oxygen molecules slide through a barrel−chromophore interface and ultimately reach the back of the chromophore, making contact with the MET part of the chromophore. These oxygen molecules remain in this region for the rest of the 30 ns simulations. Molecular oxygen entries from the bottom of the protein barrel were observed at 17 and 23 ns following a similar route as in mCherry (i.e., pocket A ↔ pocket B ↔ pocket C). Thus, the LES simulations show that the same oxygen diffusion channels in mCherry were also observed in mCherry−Q163M. However, the rate of entry as well as the number of oxygen molecules was found to be significantly higher in mCherry−Q163M as compared to mCherry, implying a correlation between reduced oxygen permeability and the improved photostability in mCherry.

In order to further investigate differences in the mechanism of oxygen diffusion, as we did with mCherry, for mCherry−Q163M we performed 20 independent simulations in which an oxygen molecule was placed just outside the protein barrel but near the chromophore (close to the gateway pocket). The initial location of the molecular oxygen is comparable to the location of the oxygen used in the mCherry simulations: the distance between the chromophore phenolic oxygen and the molecular oxygen was 2.69 Å in mCherry versus 2.70 Å in mCherry−Q163M. In the 20 runs with mCherry−Q163M, molecular oxygen was observed to enter the gateway pocket in 14 runs. In 5 of these runs, molecular oxygen diffused further into pocket C. In contrast, simulations in mCherry showed the diffusion of molecular oxygen into pocket C in only one run. Also, in mCherry−Q163M, we observed molecular oxygen making back and forth transitions between the gateway pocket and pocket C but did not observe this in mCherry.

In order to understand the structural basis for the differences in the oxygen diffusion between gateway pocket ↔ pocket C, we inspected the dynamics of the amino acid side chain involved in the interface between these pockets. The crucial side chain at the interface is residue 163, which is GLN163 in mCherry versus MET163 in mCherry−Q163M. Although the sizes of the GLN and MET side chains are quite similar, we found their dynamics to be different. In Figure 5, we plot the distribution of the dihedral angles (C−C−C−N and C−C−S−C) of GLN163 in mCherry and MET163 in mCherry−Q163M. The distributions of dihedral angles are obtained from a 25 ns window within their respective LES simulations. The dihedral angle distributions clearly show that the GLN163 side chain in mCherry is more rigid than the MET163 side chain in mCherry−Q163M. The side chain of MET163 can flip between two structures with very different peak dihedral angles of −72° and +72°. In addition, there is a probability for the MET163 side chain to assume a dihedral angle of 180°, which is not observed for GLN163. Although a combination of chromophore positions and the position of nearby atoms plays a role in the gateway pocket ↔ pocket C oxygen transitions, a number of such oxygen transitions was observed when the dihedral angle was close to 180°. We also observed that the mutation at 163 causes the rearrangement of nearby residues, such as a shift in the dihedral angle distribution of MET97, which might alter other oxygen diffusion pathways.

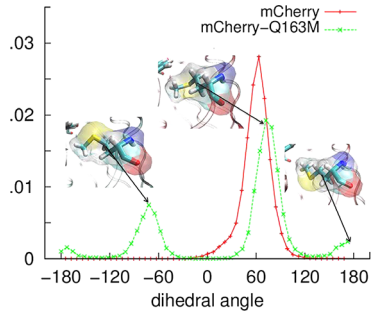

Figure 5. Distribution and schematic of side chain dihedral angles for the gateway residue GLN163 in mCherry versus MET163 in mCherry−Q163M. The MET163 is much more flexible and is more likely to allow diffusion of molecular oxygen into the protein compared to the more rigid GLN163.

CONCLUSIONS

Access for molecular oxygen to get inside the protein barrel is required for chromophore maturation in fluorescent proteins. However, oxygen access can also cause irreversible photobleaching and significantly reduce the photostabilty of an FP. In this work, we performed molecular dynamics simulations to investigate the diffusion of molecular oxygen into the protein barrel of the monomeric RFP variant mCherry. A clear channel for oxygen diffusion into the protein is described, and the free-energy of an oxygen molecule at any point along the path is calculated. The pathway contains several oxygen hosting pockets, which are identified by the amino acid residues that form each pocket. One end of the channel is accessed from the solvent through the floppy $\beta7-\beta10$ gap, which leads immediately to a gateway pocket that provides some access to the chromophore. Diffusion of molecular oxygen deeper into the protein, providing better access to the chromophore, is hindered by GLN163, but our calculations show that it becomes easier upon the mutation Q163M, which is consistent with experimental observations of significantly lower photostability for mCherry−Q163M as compared to that of mCherry. Another entrance from the solvent is at the bottom of the protein barrel and leads through other pockets to join the same pocket next to the chromophore. The oxygen access to the chromophore through regions close to $\beta7$ not only leads to collisional quenching but also affects the protein's fluorescence lifetime. Such computational identifications of oxygen diffusion pathways can be helpful in guiding mutagenesis efforts to design fluorescent proteins with improved photophysical properties.

ASSOCIATED CONTENT

Supporting Information

Movie S1 shows the molecular oxygen diffusing through pocket C and escaping the protein barrel. Movie S2 shows molecular oxygen diffusing through the $\beta7-\beta10$ gate into pocket C. This material is available free of charge via the Internet at http://pubs.acs.org.

dx.doi.org/10.1021/jp308366y | J. Phys. Chem. B 2013, 117, 2247−2253

AUTHOR INFORMATION

Corresponding Author

*E-mail: chapagap@fiu.edu. Phone: (305) 348 6266. Fax: (305) 348 6700.

Notes

The authors declare no competing financial interest.

ACKNOWLEDGMENTS

Research reported in this publication was supported by the National Institute of General Medical Sciences of the National Institutes of Health under award number SC3GM096903. The content is solely the responsibility of the authors and does not necessarily represent the official views of the National Institutes of Health. We would like to thank Professor Ralph Jimenez at JILA (University of Colorado at Boulder) for helpful discussions.

REFERENCES

(1) Tsien, R. Y. The Green Fluorescent Protein. *Annu. Rev. Biochem.* **1998**, *67*, 509−544.
(2) Zimmer, M. Green Fluorescent Protein (GFP): Applications, Structure, and Related Photophysical Behavior. *Chem. Rev.* **2002**, *102*, 759−781.
(3) Chalfie, M.; Tu, Y.; Euskirchen, G.; Ward, W. W.; Prasher, D. C. Green Fluorescent Protein As a Marker for Gene Expression. *Science* **1994**, *263*, 802−805.
(4) Shaner, N. C.; Campbell, R. E.; Steinbach, P. A.; Giepmans, B. N.; Palmer, A. E.; Tsien, R. Y. Improved Monomeric Red, Orange and Yellow Fluorescent Proteins Derived from Discosoma Sp. Red Fluorescent Protein. *Nat. Biotechnol.* **2004**, *22*, 1567−1572.
(5) Lin, M. Z.; McKeown, M. R.; Ng, H. L.; Aguilera, T. A.; Shaner, N. C.; Campbell, R. E.; Adams, S. R.; Gross, L. A.; Ma, W.; Alber, T.; Tsien, R. Y. Autofluorescent Proteins with Excitation in the Optical Window for Intravital Imaging in Mammals. *Chem. Biol.* **2009**, *16*, 1169−1179.
(6) Campbell, R. E.; Tour, O.; Palmer, A. E.; Steinbach, P. A.; Baird, G. S.; Zacharias, D. A.; Tsien, R. Y. A Monomeric Red Fluorescent Protein. *Proc. Natl. Acad. Sci.* **2002**, *99*, 7877−7882.
(7) Baird, G. S.; Zacharias, D. A.; Tsien, R. Y. Biochemistry, Mutagenesis, and Oligomerization of DsRed, a Red Fluorescent Protein from Coral. *Proc. Natl. Acad. Sci.* **2000**, *97*, 11984−11989.
(8) Merzlyak, E. M.; Goedhart, J.; Shcherbo, D.; Bulina, M. E.; Shcheglov, A. S.; Fradkov, A. F.; Gaintzeva, A.; Lukyanov, K. A.; Lukyanov, S.; Gadella, T. W.; Chudakov, D. M. Bright Monomeric Red Fluorescent Protein with an Extended Fluorescence Lifetime. *Nat. Methods* **2007**, *4*, 555−557.
(9) Subach, F. V.; Verkhusha, V. V. Chromophore Transformations in Red Fluorescent Proteins. *Chem. Rev.* **2012**, *112*, 4308−4327.
(10) Shaner, N. C.; Lin, M. Z.; McKeown, M. R.; Steinbach, P. A.; Hazelwood, K. L.; Davidson, M. W.; Tsien, R. Y. Improving the Photostability of Bright Monomeric Orange and Red Fluorescent Proteins. *Nat. Methods* **2008**, *5*, 545−551.
(11) Amara, P.; Andreoletti, P.; Jouve, H. M.; Field, M. J. Ligand Diffusion in the Catalase from Proteus Mirabilis: A Molecular Dynamics Study. *Protein Sci.* **2001**, *10*, 1927−1935.
(12) Carlson, M. L.; Regan, R. M.; Gibson, Q. H. Distal Cavity Fluctuations in Myoglobin: Protein Motion and Ligand Diffusion. *Biochemistry* **1996**, *35*, 1125−1136.
(13) Bossa, C.; Anselmi, M.; Roccatano, D.; Amadei, A.; Vallone, B.; Brunori, M.; Di Nola, A. Extended Molecular Dynamics Simulation of the Carbon Monoxide Migration in Sperm Whale Myoglobin. *Biophys. J.* **2004**, *86*, 3855−3862.
(14) Lamb, D. C.; Arcovito, A.; Nienhaus, K.; Minkow, O.; Draghi, F.; Brunori, M.; Nienhaus, G. U. Structural Dynamics of Myoglobin: An Infrared Kinetic Study of Ligand Migration in Mutants YQR and YQRF. *Biophys. Chem.* **2004**, *109*, 41−58.
(15) Gibson, Q. H.; Regan, R.; Elber, R.; Olson, J. S.; Carver, T. E. Distal Pocket Residues Affect Picosecond Ligand Recombination in Myoglobin. An Experimental and Molecular Dynamics Study of Position 29 Mutants. *J. Biol. Chem.* **1992**, *267*, 22022−22034.
(16) Brunori, M.; Gibson, Q. H. Cavities and Packing Defects in the Structural Dynamics of Myoglobin. *EMBO Rep.* **2001**, *2*, 674−679.
(17) Cohen, J.; Kim, K.; King, P.; Seibert, M.; Schulten, K. Finding Gas Diffusion Pathways in Proteins: Application to O_2 and H_2 Transport in CpI [FeFe]-Hydrogenase and the Role of Packing Defects. *Structure* **2005**, *13*, 1321−1329.
(18) Feher, V. A.; Baldwin, E.; Dahlquist, F. W. Access of Ligands to Cavities within the Core of a Protein Is Rapid. *Nat. Struct. Biol.* **1996**, *3*, 516−521.
(19) Lakowicz, J. R.; Weber, G. Quenching of Protein Fluorescence by Oxygen. Detection of Structural Fluctuations in Proteins on the Nanosecond Time Scale. *Biochemistry* **1973**, *12*, 4171−4179.
(20) Nadler, W.; Stein, D. L. Biological Transport Processes and Space Dimension. *Proc. Natl. Acad. Sci.* **1991**, *88*, 6750−6754.
(21) Wang, P. H.; Blumberger, J. Mechanistic Insight into the Blocking of Co Diffusion in [NiFe]-Hydrogenase Mutants through Multiscale Simulation. *Proc. Natl. Acad. Sci.* **2012**, *109*, 6399−6404.
(22) Branchini, B. R.; Nemser, A. R.; Zimmer, M. A Computational Analysis of the Unique Protein-Induced Tight Turn That Results in Posttranslational Chromophore Formation in Green Fluorescent Protein. *J. Am. Chem. Soc.* **1998**, *120*, 1−6.
(23) Shu, X.; Shaner, N. C.; Yarbrough, C. A.; Tsien, R. Y.; Remington, S. J. Novel Chromophores and Buried Charges Control Color in mFruits. *Biochemistry* **2006**, *45*, 9639−9647.
(24) Goedhart, J.; von Stetten, D.; Noirclerc-Savoye, M.; Lelimousin, M.; Joosen, L.; Hink, M. A.; van Weeren, L.; Gadella, T. W., Jr.; Royant, A. Structure-Guided Evolution of Cyan Fluorescent Proteins Towards a Quantum Yield of 93%. *Nat. Commun.* **2012**, *3*, 751.
(25) Roy, A.; Carpentier, P.; Bourgeois, D.; Field, M. Diffusion Pathways of Oxygen Species in the Phototoxic Fluorescent Protein KillerRed. *Photochem. Photobiol. Sci.* **2010**, *9*, 1342−1350.
(26) Chapagain, P. P.; Regmi, C. K.; Castillo, W. Fluorescent Protein Barrel Fluctuations and Oxygen Diffusion Pathways in mCherry. *J. Chem. Phys.* **2011**, *135*, 235101.
(27) Brooks, B. R.; Bruccoleri, R. E.; Olafson, B. D.; States, D. J.; Swaminathan, S.; Karplus, M. Charmm: A Program for Macromolecular Energy, Minimization, and Dynamics Calculations. *J. Comput. Chem.* **1983**, *4*, 187−217.
(28) Eswar, N.; Webb, B.; Marti-Renom, M. A.; Madhusudhan, M. S.; Eramian, D.; Shen, M. Y.; Pieper, U.; Sali, A. Comparative Protein Structure Modeling Using Modeller. In *Current Protocols in Bioinformatics*; Wiley: New York, 2006; Chapter 5, Unit 5 6.
(29) Reuter, N.; Lin, H.; Thiel, W. Green Fluorescent Proteins: Empirical Force Field for the Neutral and Deprotonated Forms of the Chromophore. Molecular Dynamics Simulations of the Wild Type and S65T Mutant. *J. Phys. Chem. B* **2002**, *106*, 6310−6321.
(30) Ulrich, E.; Lalith, P.; Max, L. B.; Tom, D.; Hsing, L.; Lee, G. P. A Smooth Particle Mesh Ewald Method. *J. Chem. Phys.* **1995**, *103*, 8577−8593.
(31) Cohen, J.; Arkhipov, A.; Braun, R.; Schulten, K. Imaging the Migration Pathways for O_2, CO, NO, and Xe inside Myoglobin. *Biophys. J.* **2006**, *91*, 1844−1857.
(32) Bevis, B. J.; Glick, B. S. Rapidly Maturing Variants of the Discosoma Red Fluorescent Protein (DsRed). *Nat. Biotechnol.* **2002**, *20*, 83−87.